

Structural and Electrical Properties of Nb-substituted $\text{LiTa}_{1-x}\text{Nb}_x\text{O}_3$ (Sifat Struktur dan Elektrik bagi $\text{LiTa}_{1-x}\text{Nb}_x\text{O}_3$ yang Digantikan dengan Nb)

K.Y. BAK, K.B. TAN*, C.C. KHAW, Z. ZAINAL, P.Y. TAN & M.P. CHON

ABSTRACT

Single phase $\text{LiTa}_{1-x}\text{Nb}_x\text{O}_3$ solid solution with $0.00 \leq x \leq 1.00$ was successfully synthesised via conventional solid-state method at 950°C for 24 h. These materials were refined and fully indexed with hexagonal crystal system, space group of $R3c$; lattice parameters, a ranging from $5.1410(6) \text{ \AA}$ to $5.1471(3) \text{ \AA}$ and c ranging from $13.7467(1) \text{ \AA}$ to $13.8341(1) \text{ \AA}$; with $\alpha = \beta = 90^\circ$ and $\gamma = 120^\circ$. Variation of the lattice parameters in these materials was found to be negligibly small throughout the subsolidus solution. No thermal event was detected within the studied temperature range of 50 to 1000°C . The electrical properties of samples were characterised by AC impedance analyser, HP4192A at temperature ranging from room temperature to 850°C over a frequency range of 5 Hz to 13 MHz. $\text{LiTa}_{1-x}\text{Nb}_x\text{O}_3$ materials exhibited bulk response with associated capacitances in the order of $10^{-12} \text{ F cm}^{-1}$ and the temperature-dependent conductivities were found to increase with increasing temperatures. The results showed that $\text{LiTa}_{1-x}\text{Nb}_x\text{O}_3$ samples were of typical ferroelectrics.

Keywords: Ferroelectric; impedance; solid solution; solid-state method

ABSTRAK

Larutan pepejal $\text{LiTa}_{1-x}\text{Nb}_x\text{O}_3$ tulen dengan $0.00 \leq x \leq 1.00$ telah berjaya disintesis melalui kaedah penyediaan keadaan pepejal pada 950°C selama 24 jam. Bahan-bahan tersebut dapat diindeks sepenuhnya dalam sistem kristal heksagon dengan kumpulan ruangan, $R3c$; nilai parameter kekisi, a , b dalam julat $5.1410(6) \text{ \AA}$ ke $5.1471(3) \text{ \AA}$ dan c dalam lingkungan $13.7467(1) \text{ \AA}$ ke $13.8341(1) \text{ \AA}$; $\alpha = \beta = 90^\circ$ dan $\gamma = 120^\circ$. Perubahan parameter kekisi larutan pepejal $\text{LiTa}_{1-x}\text{Nb}_x\text{O}_3$ didapati adalah terhad. Tiada sebarang keadaan terma dikesan daripada suhu 50 sehingga 1000°C . Sifat elektrik dicirikan dengan penganalisis AC impedans, HP4192A daripada suhu bilik hingga 850°C dalam julat frekuensi antara 5 Hz hingga 13 MHz. Bahan-bahan dalam siri larutan pepejal menunjukkan sifat pukal dengan kapasitan dalam tertib $10^{-12} \text{ F cm}^{-1}$. Konduktiviti bagi sampel ini didapati meningkat dengan peningkatan suhu. Keputusan analisis menunjukkan siri larutan pepejal $\text{LiTa}_{1-x}\text{Nb}_x\text{O}_3$ dengan $0.00 \leq x \leq 1.00$ bersifat jenis bahan ferroelektrik.

Kata kunci: Ferroelektrik; impedans; kaedah penyediaan keadaan pepejal; larutan pepejal

INTRODUCTION

Lithium is well-known for its wide application in the production of batteries and this has led on to the intensive studies on those derivatives from lithium-based binary systems. Lithium cobalt oxide, LiCoO_2 , is commonly used as positive electrodes in lithium ion batteries. On the other hand, lithium titanium oxide, Li_2TiO_3 , which is the main component in rechargeable battery, provides an advantage of recharging faster than other ordinary lithium-ion batteries. The use of titanium improves the surface area of the anode compartment that allows quicker mobility of electrons and therefore, fast recharging process is possible (Karhunen et al. 2011; Yao et al. 1995).

Lithium based binary materials containing pentavalent cations, e.g. Nb and Ta are equally interesting. Oxides from lithium-tantalum and lithium-niobium systems demonstrate good dielectric properties that could be utilised in the production of optics, cell phones, motion detectors and sensors (Evans et al. 2006; He et al. 2008; Wan et al. 2002). Due to the technological interests in the aforementioned applications, much research interest

has been triggered and therefore, considerable works are performed on the crystallography and electrical properties study of these binary systems (Iyi et al. 1992; Kitamura et al. 1992).

In the binary system containing Nb, crystal structure and the possible defects are of major study focus prior to any further enhancement in the related property. Ideally, LiNbO_3 is nonstoichiometric, i.e. Li-deficient, for which evaporation of lithium during material processing at high temperature could contribute to the occurrence of this defective structure. The nonstoichiometric single crystal preferably could be grown at congruently melting composition with 48.5 mol% of Li_2O (Iyi et al. 1992; Kitamura et al. 1992). Other efforts have been made to prepare near-stoichiometric ($\text{Li}/(\text{Li} + \text{Nb}) = 0.498$) LiNbO_3 crystal in order to improve its physical and optical properties using different synthesis methods, e.g. sol-gel method and low temperature hydrothermal route (Iyi et al. 1992; Samuel et al. 2007; Zhan et al. 2011). From the viewpoint of optical properties, the stoichiometric composition is more desirable because defects introduced

in the Nb-rich composition ($\text{Li}/(\text{Li} + \text{Nb}) = 0.470$) are detrimental to the optical properties of LiNbO_3 . To understand and control the properties of LiNbO_3 , knowledge of the defect structure is therefore indispensable before any conclusive remarks could be drawn. The stoichiometric LiNbO_3 is found to be pure hexagonal phase with space group of $R3c$ and a wide range of dopants including from +1 valent state to the +3 valent state rare earth cations could possibly be introduced into this crystal structure (Megaw 1968; Xue et al. 2000). The influence of various dopants on the physicochemical, ferroelectric and structural characteristics of lithium niobate single crystals has been investigated in which low concentration rare earth cationic dopants are expected to localise in the regular Li octahedra. However, increased dopant concentration could lead to an essential complication of the rare earth localisation scheme, presumably due to the formation of different clusters, change of local environment or even position of the cationic dopants introduced (Palatnikova et al. 2006). It is noteworthy that loss tangents in most ferroelectrics are found to increase with the increasing frequency ranging from microwave to millimeter-wave. Such increment may be attributed to the temporal response limitations of both intrinsic unit cell polarisation and also extrinsic charged defects to an applied oscillating electric field (Mark 2001).

In the case of Ta analogue, the crystal structure for congruent LiTaO_3 is determined to be of trigonal cell with $a = 5.154 \text{ \AA}$ and $c = 13.7808 \text{ \AA}$ (Abrahams et al. 1966). A second order phase transition is observed for a high temperature paraelectric phase with space group symmetry of $R3c$ from a ferroelectric phase of symmetry $R3c$ at Curie temperature, T_c of $\sim 1190^\circ\text{C}$ (Ballman & Brown 1972). Such transition gives rise to a loss of inversion symmetry at the transition point of which a spontaneous polarisation along the polar c axis is developed. The distorted oxygen octahedra are connected together by common faces along the c axis, constructing equidistant oxygen layers perpendicular to the c axis with distance of $c/6$. Note that both Li and Ta have been found to displace 0.60 \AA and 0.20 \AA along the same crystallographic axis and such displacements have created dipole moments that required for spontaneous polarisation within the structure. This material has been claimed to have a net spontaneous ferroelectric polarisation, P_s , oriented along the c axis as adjacent neighbouring Li^+ - Ta^{5+} pair is arranged in a specific pattern along the trigonal axis (Hsu et al. 1997). Similarly, various dopants, e.g. rare earth cations (Nd, Ho, Tm, Yb, Pr) and transition metal ions (Cu, Cr) have been introduced into the lithium tantalate system of which LiTaO_3 single crystal is expected to exhibit better optical properties (Kaczmarek et al. 2000). On the other hand, dielectric and ferroelectric properties of multilayer lithium tantalate thin films prepared by sol-gel technique have been reported by Satapathy et al. (2011). These polycrystalline films are found to exhibit low dielectric constant, 6.4 at 10 kHz and remnant polarisation, $1.5 \mu\text{C}/\text{cm}^2$ at an applied voltage of $100 \text{ kV}/\text{cm}$.

Considering the close similarity of chemical properties and identical cationic size, Nb has been selected as a dopant in an attempt to enhance the electrical properties of the ceramic samples in lithium tantalate binary system. The aims of this paper were to discuss our findings on the subsolidus solution formation and AC electrical response of Nb substituted lithium tantalates.

EXPERIMENTAL DETAILS

High purity grade of Li_2CO_3 (99%, Aldrich), Ta_2O_5 (99%, Aldrich) and Nb_2O_5 (99%, Aldrich) were used as starting materials for the synthesis of $\text{LiTa}_{1-x}\text{Nb}_x\text{O}_3$. Oxides were treated at different pre-firing temperatures prior to weighing and further solid-state reaction. Stoichiometric amount of oxides were weighed out, ground homogeneously with sufficient acetone and then transferred into alumina boat before step-wise heat treatment. The mixtures were allowed to react at initial temperatures of 300 and 600°C for 2 h, respectively; whilst, the firing condition was finalised at 950°C for 24 h in muffle furnace. Intermediate regrinding was performed in order to refresh surface area for better reactivity. Phase purities of the prepared samples were investigated by Shimadzu x-ray powder diffractometer (XRD) 6000, which was equipped with a diffracted beam graphite monochromator, $\text{CuK}\alpha$ radiation, 1.5418 \AA at a routine scan rate of $2^\circ/\text{min}$. Lattice parameter refinement was performed using *CheKcell* software using XRD data that collected at slow scan rate of $0.1^\circ/\text{min}$. The thermal stability of phase pure samples was examined by Perkin Elmer thermal gravimetry analyser (TGA 7). Fourier-transform infrared spectroscopy (FT-IR) was performed on single phase materials for structural analysis. The surface morphologies of the samples were examined by scanning electron microscopy (SEM, JOEL JSM-6400).

Pellets with thickness of approximately 1.0 - 2.0 mm were prepared by a stainless steel die of 8 mm in diameter. The Engelhard gold paste were applied on both sides of the pellet, and then dried in a furnace from 200 to 600°C at a heating rate of $1^\circ\text{C}/\text{min}$. The organometallic paste was evaporated and hardened to act as the electrodes before further electrical property analysis using AC (alternating current) impedance analyser, HP 4192A. The measurements over a frequency range of 5 Hz - 13 MHz were performed in heat-cool cycle in temperature range of ~ 30 to 850°C with incremental steps of 50°C and equilibration time of 25 min .

RESULTS AND DISCUSSION

Samples with a general formula of $\text{LiTa}_{1-x}\text{Nb}_x\text{O}_3$, where $x = 0.00$ to 1.00 , have been synthesised by conventional solid-state method at the firing temperature of 950°C for 24 h. Phase identification of the prepared samples is performed by X-ray diffraction analysis in which their XRD spectra are compared with the standard reference of International Crystal Diffraction Data (ICDD) card number 029-0836. All XRD diffraction spectra are combined as shown in

Figure 1. No additional characteristic diffraction peaks are discernible confirming that a complete substitutional solid solution, $\text{LiTa}_{1-x}\text{Nb}_x\text{O}_3$ ($0.00 \leq x \leq 1.00$) has been formed. This result agrees reasonably well with those reported in literature (Gervais & Fonseca 1997; Xue et al. 2000). The solid solutions are found to crystallise in a hexagonal crystal symmetry, R3c space group, $a = b \neq c$, $\alpha = \beta = 90^\circ$; $\gamma = 120^\circ$ with their lattice parameters in the range of $5.1410(6) \text{ \AA} \leq a \leq 5.1471(3) \text{ \AA}$ and $13.7467(1) \text{ \AA} \leq c \leq 13.8341(1) \text{ \AA}$, respectively. All XRD diffraction planes are fully indexed and there is hardly any significant cell expansion, i.e. little variation in terms of their a -, b - axes and c - axis is observed in Nb substituted lithium tantalates. This is further ascertained by their XRD spectra of which all peaks of this subsolidus solution are in plane to one another over full 2 theta range. It is worthwhile to highlight that peak position and d-spacing are well correlated through Bragg's Law and a shift in 2θ would be anticipated if significant change in lattice parameter has occurred.

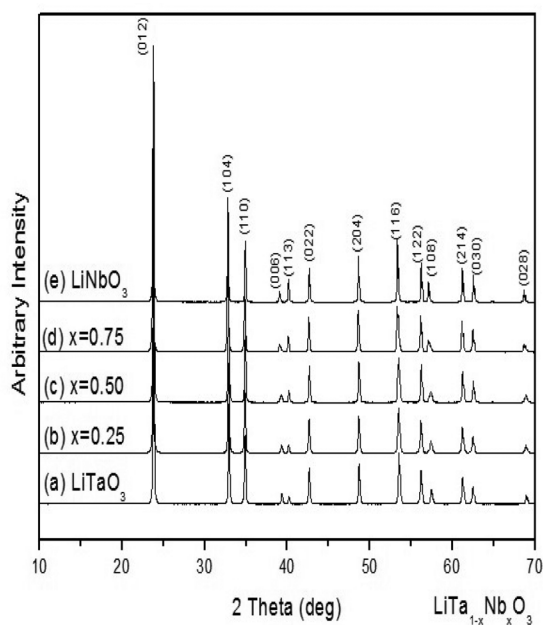


FIGURE 1. XRD patterns of (a) LiTaO_3 , (b) $\text{LiTa}_{0.75}\text{Nb}_{0.25}\text{O}_3$, (c) $\text{LiTa}_{0.5}\text{Nb}_{0.5}\text{O}_3$, (d) $\text{LiTa}_{0.25}\text{Nb}_{0.75}\text{O}_3$, (e) LiNbO_3 prepared via conventional solid-state method at the firing temperature of 950°C over 24 h

The formation of $\text{LiTa}_{1-x}\text{Nb}_x\text{O}_3$ solid solution is proposed to be a direct replacement of Ta by Nb through substitutional mechanism. Nb^{5+} dopant is introduced directly to replace Ta^{5+} cation as no charge compensation will be required in order to preserve the overall electroneutrality of the system (West 1999). Meanwhile, the identical cationic radii of Nb^{5+} and Ta^{5+} of 0.78 \AA under a six-fold coordination environment is of much help for the subsolidus formation (Ekhelikar & Bichile 2004). In addition to this, both end members, LiNbO_3

and LiTaO_3 are isostructural and this allows a full range of dopant to be successfully incorporated within the prepared compositions.

On the other hand, lattice parameters of $\text{LiTa}_{1-x}\text{Nb}_x\text{O}_3$ solid solution ($0.00 \leq x \leq 1.00$) were obtained through structural refinement using *Chekkcell* program. The recorded lattice parameters against composition, x in $\text{LiTa}_{1-x}\text{Nb}_x\text{O}_3$ are shown in Figure 2, respectively. It is observed that variation of lattice parameters is negligibly small implying that the size of unit cell remains similar and this again, provides additional evidence for the aforementioned explanation on their identical cationic radii. The increment or decrement of lattice constants within a solid solution is usually governed by the size of ions if the structure does not undergo distinct phase changes or experience any possible structural strain. It is apparent that an almost linear increment of c -axis has fulfilled the Vegard's law showing a slightly elongated plane along c axis. This is favourable for compositions with higher Nb content in order to accommodate the possible cationic displacement. Notably, the structure of LiTaO_3 generally consists of layers of distorted oxygen octahedral containing center cation, i.e. Li or Ta that perpendicular to c axis with distance of $c/6$. Both Li^+ and Ta^{5+} had been claimed to displace from their ideal positions (Hsu et al. 1997). Such phenomenon may have arisen due to the fact that Li^+ is considerably too small to fit into a six-fold coordinated site.

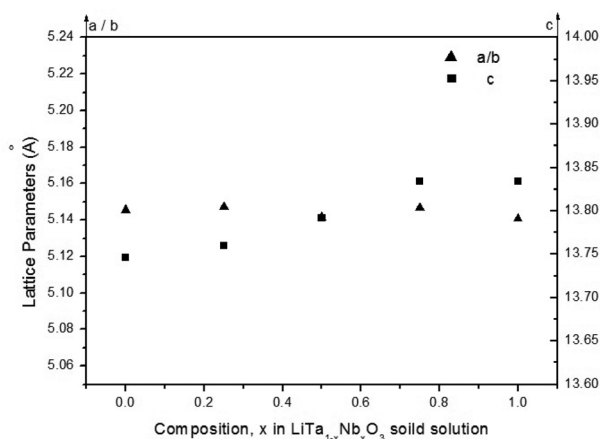


FIGURE 2. Lattice parameters versus composition, x in $\text{LiTa}_{1-x}\text{Nb}_x\text{O}_3$ solid solution ($0.00 \leq x \leq 1.00$) with $5.1410(6) \text{ \AA} \leq a, b \leq 5.1471(3) \text{ \AA}$ and $13.7467(1) \text{ \AA} \leq c \leq 13.8341(1) \text{ \AA}$

Scherrer and Williamson-Hall (W-H) methods were introduced to calculate the crystallite sizes of compositions in $\text{LiTa}_{1-x}\text{Nb}_x\text{O}_3$ subsolidus solution. These methods rely on XRD data in which the crystallite size is correlated to the broadening of an intense diffraction peak. Both equations are denoted in (1) and (2), respectively.

$$\tau = \frac{K\lambda}{\beta \cos\theta}, \quad (1)$$

where τ , K , λ , β , and θ correspond to the mean size of the ordered crystallite domains, dimensionless shape factor, X-ray wavelength, full width at half maximum (FWHM) of the most intense peak and Bragg angle, respectively.

$$\beta \cos \theta = \frac{K\lambda}{D} + 4\varepsilon \sin \theta, \quad (2)$$

where β , θ , K , λ , D and ε are parameters referring to full width at half maximum (FWHM) for line broadening, Bragg angle, dimensionless shape factor, x-ray wavelength, crystallite size and internal strain, respectively.

The calculated crystallite sizes for the subsolidous solution series of $\text{LiTa}_{1-x}\text{Nb}_x\text{O}_3$ are tabulated in Table 1, while the internal strain plot is shown in Figure 3. Note that there is no strong correlation between the results obtained from both methods; however, the determined crystallites are found in the range of ~45-90 nm, which is much smaller than the determined grain sizes by SEM analysis. The internal strain is found to decrease with the increased Nb concentration which indicates the slightly elongated structure has stronger flexibility to accommodate higher dopant concentration. On the other hand, no thermal event associated with weight changes is discernible in the resultant thermograms within the studied temperature range (Figure 4) as the prepared samples of $\text{LiTa}_{1-x}\text{Nb}_x\text{O}_3$ solid solutions ($0.00 \leq x \leq 1.00$) are thermally stable and impervious to any thermal changes. However, some $\text{LiTa}_{1-x}\text{Nb}_x\text{O}_3$ ($0 \leq x \leq 1.0$) samples have experienced a tiny weight

TABLE 1. The calculated crystallite sizes of $\text{LiTa}_{1-x}\text{Nb}_x\text{O}_3$ solid solution using Scherrer and Williamson-Hall methods

x	Size of crystallites (nm)	
	Scherrer method	W-H method
0.00	50.78	81.82
0.25	53.10	90.00
0.50	50.78	64.29
0.75	54.16	69.23
1.00	60.63	45.00

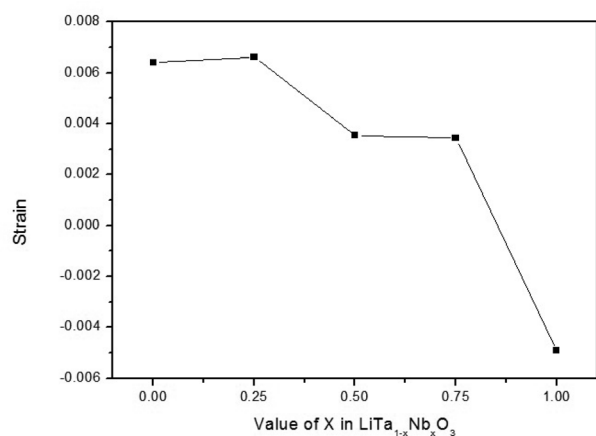


FIGURE 3. Internal strain plot of $\text{LiTa}_{1-x}\text{Nb}_x\text{O}_3$ samples using Williamson-Hall method

gain at the starting temperature and this phenomenon is common for oxide ceramics.

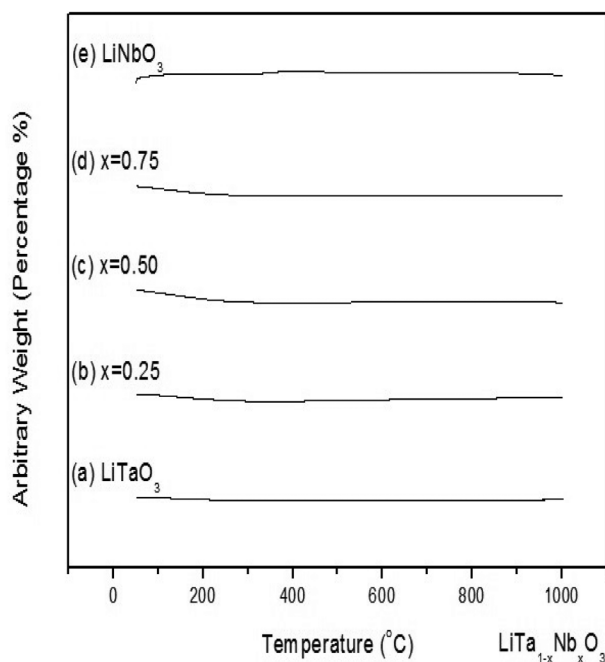


FIGURE 4. TGA thermograms of $\text{LiTa}_{1-x}\text{Nb}_x\text{O}_3$ solid solution ($0.00 \leq x \leq 1.00$)

SEM micrographs of $\text{LiTa}_{1-x}\text{Nb}_x\text{O}_3$ solid solution ($0.00 \leq x \leq 1.00$) are recorded at a magnification of 5k (Figure 5). The microstructures of these samples contained grains of various shapes. It is observed that a consistent increase of grain size is accounted for samples with increased Nb content (Table 2). Grain sizes of the prepared samples are determined in a range of 0.56 - 6.33 μm which indicates the larger grains are composed of hundreds of smaller crystallites. Meanwhile, the consistent grain growth is probably due to lower crystallisation temperature of the niobium oxide with a melting point of 1512°C if compared to that of tantalum, 1872°C (Wachs et al. 2000). The change in grain size of each composition could probably have a significant impact on activation energy and the magnitude of electrical conductivity. Electronic transport property in samples with large grain sizes could have varied especially the space charge potential is of an important factor to be considered (Gopalan et al. 2001).

In contrast to organic compounds, inorganic solids tend to absorb infrared light at lower wave number region, which is usually below 1000 cm^{-1} at ambient temperature. The IR absorption bands in the range of 100-300 cm^{-1} are usually assigned to vibrations of ions in the crystal lattice due to any translational or rotational motion. However, there is such possibility that the absorption bands may occur at higher wave numbers due to some combination of ions with different fundamental modes. The infrared active modes that are attributed to the bending and stretching vibrations of metal oxygen bonds are possibly

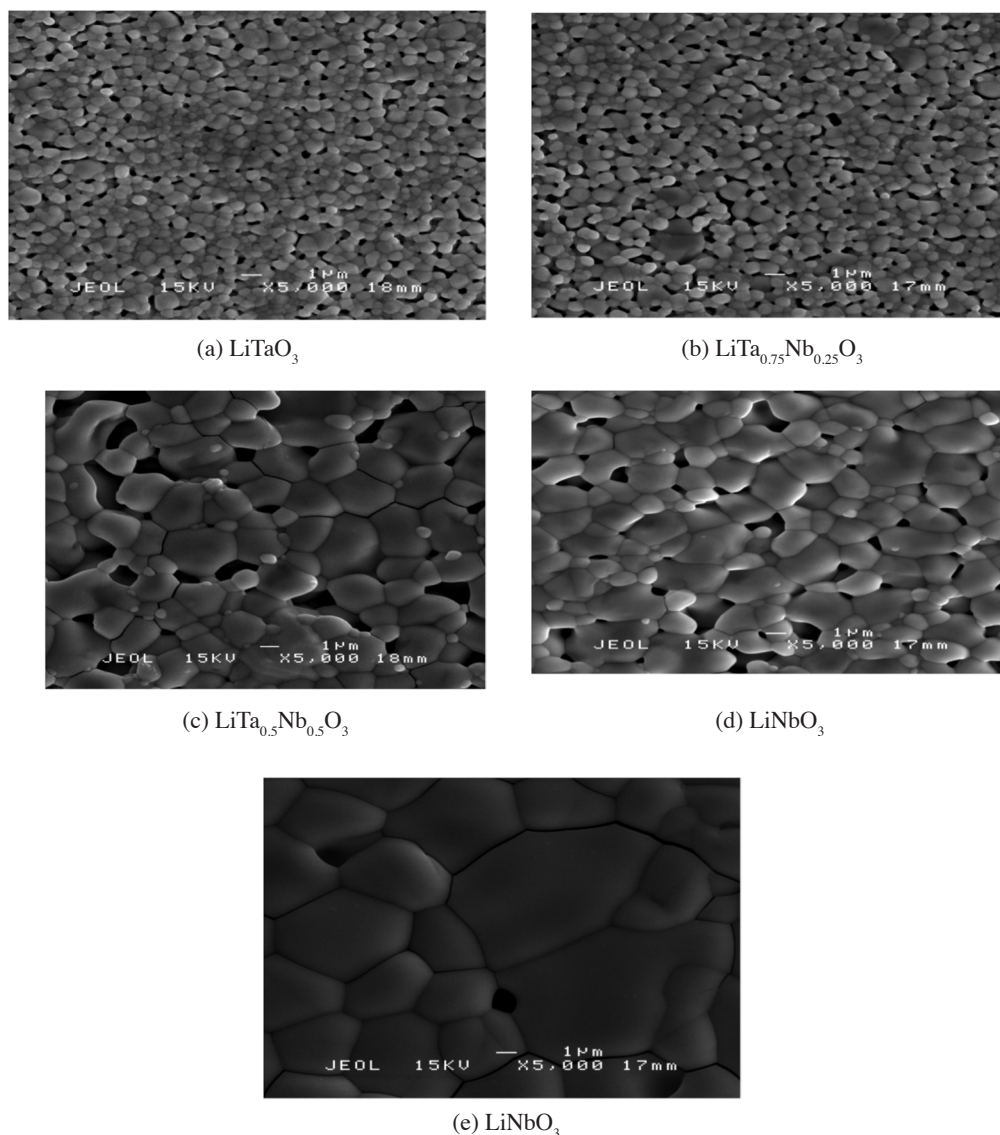


FIGURE 5. SEM micrographs of $\text{LiTa}_{1-x}\text{Nb}_x\text{O}_3$ solid solution ($0.00 \leq x \leq 1.00$) at a magnification of 5000 \times

TABLE 2. The determined grain size of $\text{LiTa}_{1-x}\text{Nb}_x\text{O}_3$ solid solution ($0.00 \leq x \leq 1.00$)

x	Range of grain size (μm)
0.00	0.56 - 1.33
0.25	0.56 - 1.89
0.50	0.56 - 3.22
0.75	0.78 - 3.44
1.00	3.22 - 6.33

be characterised using infrared spectroscopy (Griffiths & Haseth 2007). Figure 6 shows the IR absorption spectra of $\text{LiTa}_{1-x}\text{Nb}_x\text{O}_3$ solid solution ($0.00 \leq x \leq 1.00$) and the summary of observed phonon modes is tabulated in Table 3. Constant shifts are observed in the regions of 546-576 cm^{-1} and 350-368 cm^{-1} , respectively. It is noted that these peaks occur at a decreasing wave number with a constant increase of Nb concentration. Such phenomenon could

be well explained by Hooke's Law (3) of which wave numbers or stretching vibration frequencies (ν) is directly proportional to the mass of bonding atoms.

$$\nu = \frac{\pi c}{2} \sqrt{\frac{k}{\mu}}, \quad (3)$$

where ν , c , k and μ correspond to wave number (cm^{-1}), velocity of light (cm s^{-1}) force constant (dynes cm^{-1}) and reduced mass of atoms (g), respectively.

Considering atomic weight of Ta, 180.95 g/mol which is nearly two-fold heavier than that of Nb, 92.91 g/mol, stretching vibration of Ta-O (B-O) bond is therefore expected to happen at a higher wave number region. Meanwhile, another absorption band is observed at the region of around 307 cm^{-1} , which belongs to the A-O bond stretching of Li-O. Unlike the constant shift pattern in the B-O bond stretching of Ta/Nb-O, the absorption band has

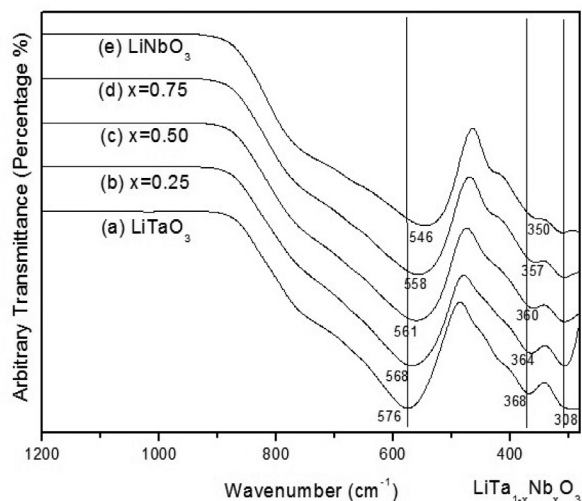


FIGURE 6. IR absorption spectra of $\text{LiTa}_{1-x}\text{Nb}_x\text{O}_3$ solid solution ($0.00 \leq x \leq 1.00$)

been consistent regardless of the change in $\text{LiTa}_{1-x}\text{Nb}_x\text{O}_3$ composition. The phenomenon is right to expectation as the composition of Li-O remains constant throughout the subsolidus solution.

Conductivity values of the samples are extracted from the high intercept of each complex Cole-Cole plot, i.e. at

TABLE 3. Summary of the observed phonon modes of $\text{LiTa}_{1-x}\text{Nb}_x\text{O}_3$ solid solution ($0.00 \leq x \leq 1.00$)

Sample	Wavenumbers (cm^{-1})		
LiTaO_3	576	368	307
$\text{LiTa}_{0.75}\text{Nb}_{0.25}\text{O}_3$	568	364	307
$\text{LiTa}_{0.50}\text{Nb}_{0.50}\text{O}_3$	561	360	308
$\text{LiTa}_{0.25}\text{Nb}_{0.75}\text{O}_3$	558	357	307
LiNbO_3	546	350	308

$Z'' = 0$ (Figure 7). The plots of $\text{LiTa}_{1-x}\text{Nb}_x\text{O}_3$ solid solution ($0.00 \leq x \leq 1.00$) could form complete semicircles at high temperatures, i.e. above 750°C that correspond to bulk resistivities. As the temperature decreases to below 750°C , incomplete semicircles are noticeable at low frequency region as these materials appear to be too resistive. Composition, $\text{LiTa}_{0.50}\text{Nb}_{0.50}\text{O}_3$ is chosen for further discussion as it should contain properties of both Ta and Nb analogues. Bulk resistivities, R_b of $\text{LiTa}_{0.50}\text{Nb}_{0.50}\text{O}_3$ are $1.92 \times 10^5 \text{ ohm cm}$ and $8.49 \times 10^4 \text{ ohm cm}$ at 800°C and 850°C , respectively. A drop in resistivities could be attributed to the increase of thermally activated charge carriers or possible local structure destruction that allows alternative low-conductivity pathway. At 850°C , an associated

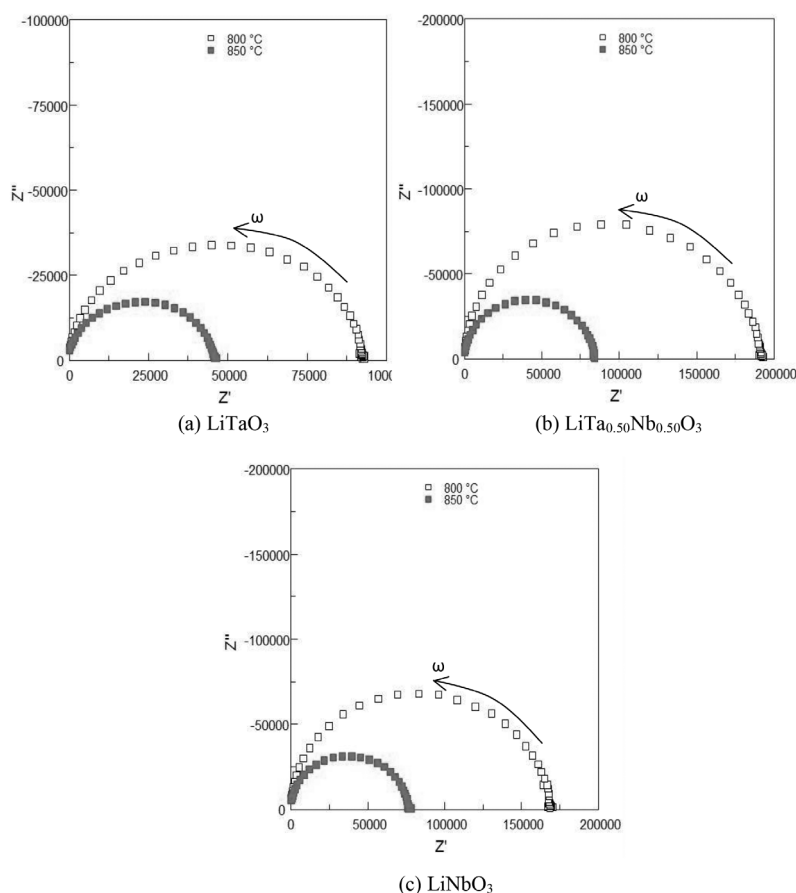


FIGURE 7. Complex Cole-Cole plots of (a) LiTaO_3 , (b) $\text{LiTa}_{0.50}\text{Nb}_{0.50}\text{O}_3$ and (c) LiNbO_3 at the temperatures of 800 and 850°C , respectively

capacitance value of $6.41 \times 10^{-12} \text{ F cm}^{-1}$ is calculated at the maximum point of the semicircle, i.e. $\omega_{\text{max}} RC = 1$ (4). This value falls in the pF range and the electrical response is therefore attributed to the bulk response (Irvine et al. 1990). Summary of the bulk resistivities, R_b and conductivities, σ of LiTaO_3 , $\text{LiTa}_{0.50}\text{Nb}_{0.50}\text{O}_3$ and LiNbO_3 at both 800 and 850°C is tabulated in Table 4.

Figure 8 shows the frequency maxima of Z'' and M'' are slightly deviated for $\text{LiTa}_{0.50}\text{Nb}_{0.50}\text{O}_3$ at both temperatures of 800 and 850°C. The measured magnitudes of full width at half maximum (FWHM) of the M'' peaks of $\text{LiTa}_{0.50}\text{Nb}_{0.50}\text{O}_3$ are approximately 1.30 decades and 1.36 decades implying that this material is not perfectly homogeneous in their electrical response (Khaw et al. 2008). The Arrhenius-type thermally activated electrical conduction of $\text{LiTa}_{1-x}\text{Nb}_x\text{O}_3$ solid solution is demonstrated in Figure 9 (Tan et al. 2012). A gradual decrease in conductivity is observed from the electrical data at higher temperature region to lower temperature region. The activation energies of the $\text{LiTa}_{1-x}\text{Nb}_x\text{O}_3$ solid solution have been calculated from the slopes of Figure 9 and then tabulated in Table 5. The values are found to be fluctuating throughout the series, with the highest activation energy of 0.68 eV at $x=0.25$.

On the other hand, modulus spectra, M'' versus frequency on a logarithmic scale from 600 to 850°C (Figure 10) show decreasing peak height at elevated temperatures.

The maxima of the curves are found to shift towards higher frequency region with increasing temperature indicating a substantial gain in capacitance, since (5). It is worthwhile to highlight that ferroelectric materials are characterised by the hysteresis of polarisation below the Curie temperature, T_c especially an order-disorder phase transition had been reported in LiTaO_3 of which the dipole moment created from disordered structure at high temperatures could give rise to higher capacitance (Seshadri et al. 2008).

The temperature dependence and frequency dependence of dielectric properties of $\text{LiTa}_{1-x}\text{Nb}_x\text{O}_3$ solid solution ($0.00 \leq x \leq 1.00$) were studied at various frequencies and temperatures. High dispersion behavior of the real part of complex permittivity, ϵ' is observed for $\text{LiTa}_{0.50}\text{Nb}_{0.50}\text{O}_3$ at low frequency region; whilst, the magnitudes of ϵ' become frequency-independent at high frequency region (Figure 11). The consistent increase of ϵ' values at higher temperatures are agreed reasonably with the aforementioned behavior of electric modulus, M'' . Figure 12 shows the temperature dependence of the dielectric constant, ϵ' of $\text{LiTa}_{0.50}\text{Nb}_{0.50}\text{O}_3$ at selected frequencies, e.g. 10 kHz, 100 kHz and 1 MHz. At temperatures below 600°C, ϵ' values are found to increase regardless of frequency; however, a higher degree of dispersion in ϵ' is discernible for frequency of 10 kHz at higher temperatures. The observed phenomenon here is probably attributed to the rapid change in AC electric

TABLE 4. Summary of the bulk resistivities, R_b and conductivities, σ of LiTaO_3 , $\text{LiTa}_{0.50}\text{Nb}_{0.50}\text{O}_3$ and LiNbO_3 at 800 and 850°C

Sample	Temperature (°C)	Bulk resistivities, R_b (ohm cm)	Bulk conductivity, σ (S cm^{-1})
LiTaO_3	800	9.25×10^4	1.08×10^{-5}
	850	4.72×10^4	2.12×10^{-5}
$\text{LiTa}_{0.50}\text{Nb}_{0.50}\text{O}_3$	800	1.92×10^5	5.21×10^{-6}
	850	8.49×10^4	1.18×10^{-5}
LiNbO_3	800	1.71×10^5	5.85×10^{-6}
	850	7.72×10^4	1.30×10^{-5}

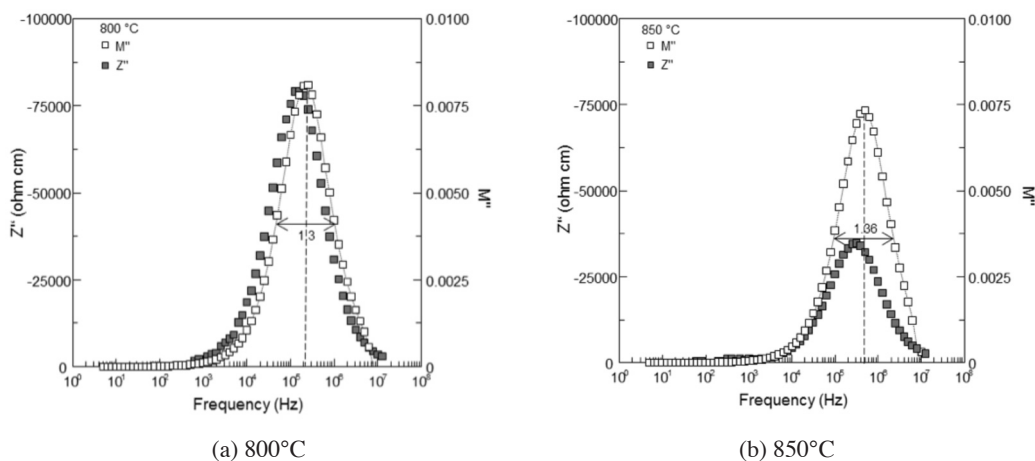


FIGURE 8. Combined Z'' and M'' spectroscopic plots of $\text{LiTa}_{0.50}\text{Nb}_{0.50}\text{O}_3$ showing FWHM values of 1.30 decades at (a) 800°C and 1.36 decades at (b) 850°C, respectively

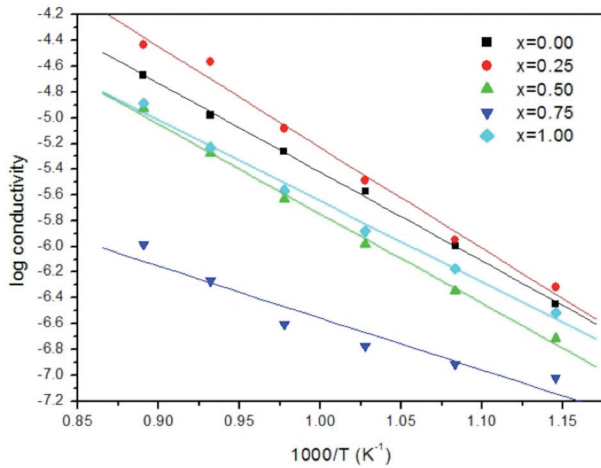


FIGURE 9. Arrhenius conductivity plots of $\text{LiTa}_{1-x}\text{Nb}_x\text{O}_3$ solid solution ($0.00 \leq x \leq 1.00$) from 600 to 850°C (cooling cycle)

TABLE 5. Summary of the determined activation energies of $\text{LiTa}_{1-x}\text{Nb}_x\text{O}_3$ solid solution

x	Activation energy (eV)
0.00	0.60
0.25	0.68
0.50	0.60
0.75	0.35
1.00	0.54

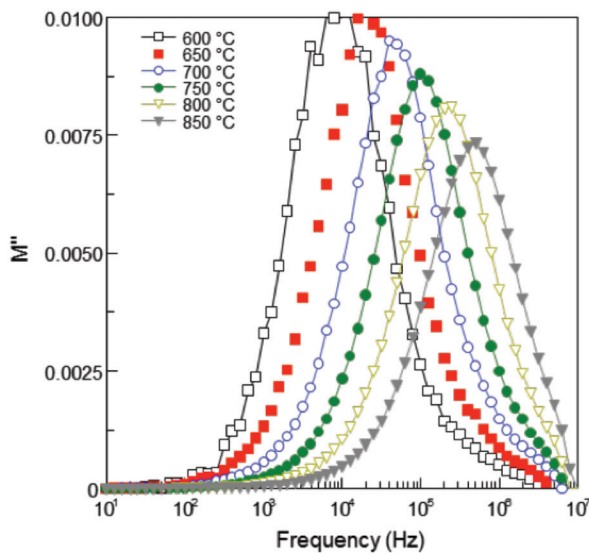


FIGURE 10. Variation of the imaginary part of modulus, M'' of $\text{LiTa}_{0.50}\text{Nb}_{0.50}\text{O}_3$ as a function of frequency from 600 to 850°C (cooling cycle)

field in which the charge carriers are unable to exchange with metal electrode and therefore, their ϵ' contribution is reduced.

Figure 13 illustrates the dielectric losses, $\tan \delta = \epsilon''(\omega) / \epsilon'(\omega)$ (6) as a function of frequency. A dense and

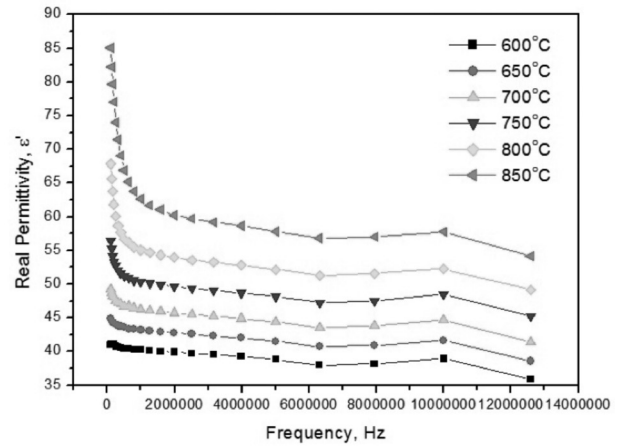


FIGURE 11. Real part of the complex permittivity, ϵ' of $\text{LiTa}_{0.50}\text{Nb}_{0.50}\text{O}_3$ as a function of frequency from 600 to 850°C

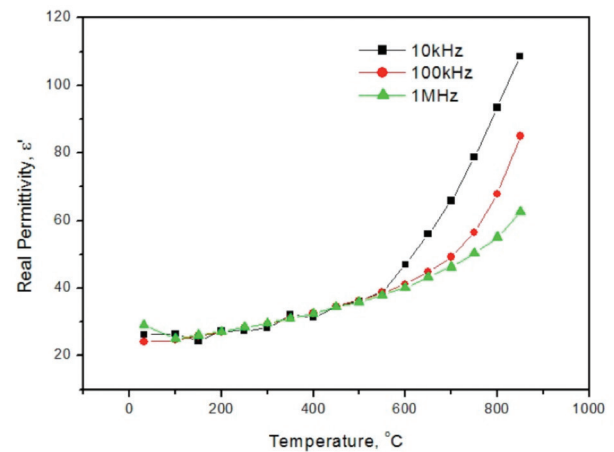


FIGURE 12. Real part of the complex permittivity, ϵ' of $\text{LiTa}_{0.50}\text{Nb}_{0.50}\text{O}_3$ as a function of temperature for various frequencies at 10 kHz, 100 kHz and 1 MHz

low pore structure is a prerequisite required for low loss dielectric as the pores may take up extra moisture which could result in an increase of loss when the soluble ions are released from the solid phase (Khaw et al. 2008; Tan et al. 2012). All the curves display a downward feature of the dielectric losses from higher frequency to lower frequency but little variation is found in the dielectric losses once frequency achieve above 1 MHz. Similar trend of dielectric loss is observed for all temperatures in the fixed-frequency format of dielectric loss of $\text{LiTa}_{0.50}\text{Nb}_{0.50}\text{O}_3$ in which higher dielectric loss recorded at the temperature of 850°C could probably due to the influx of thermally activated charge carriers. The high dielectric losses at low frequency region could be attributed to the screening charge effect in which the energy is lost during electrical conduction. As the frequency increases, lower polarisation could give rise to a near-to-linear dielectric loss at high frequency region (Mark 2001). At fixed frequency of 10 kHz, the dielectric loss increases exponentially with an increase of

temperature; whilst, a nearly non-temperature dependent dielectric loss is observed for frequency of 1 MHz (Figure 14). Such phenomenon is again can be associated with the time availability during rapid shift of the potential sign in AC electric field at high frequency.

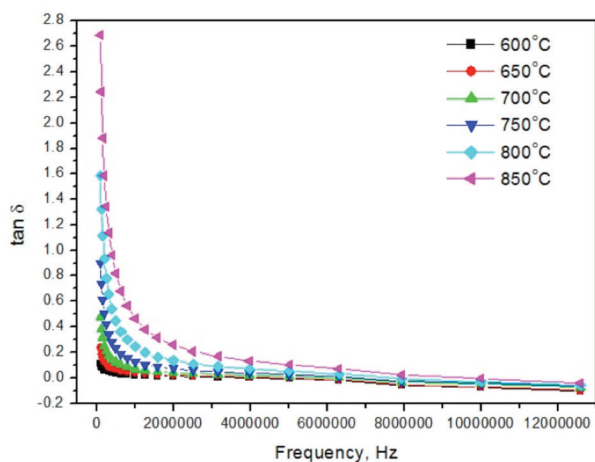


FIGURE 13. Dielectric loss, $\tan \delta$ of $\text{LiTa}_{0.50}\text{Nb}_{0.50}\text{O}_3$ as a function of frequency from 600 to 850°C

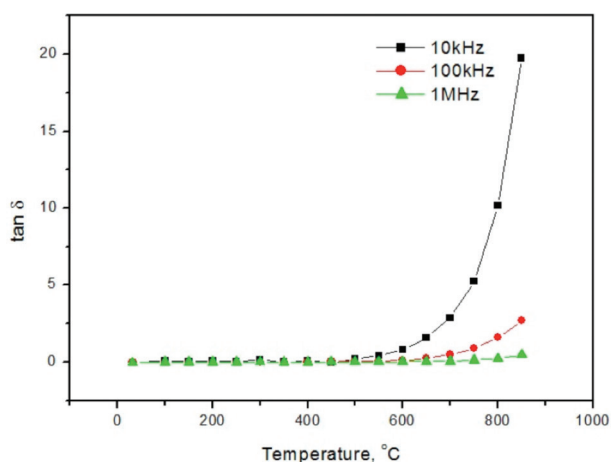


FIGURE 14. Dielectric loss, $\tan \delta$ of $\text{LiTa}_{0.50}\text{Nb}_{0.50}\text{O}_3$ as a function of temperature for 10 kHz, 100 kHz and 1 MHz

CONCLUSION

A complete solid solution of Nb substituted lithium tantalates had been successfully synthesised through conventional solid state method at the firing temperature of 950°C over 24 h. Little variation of the refined lattice parameters indicated negligibly small cell expansion due to the close ionic radii size. The thermally stable $\text{LiTa}_{1-x}\text{Nb}_x\text{O}_3$ solid solution was impervious to any thermal event showing bulk electrical response with an associated capacitance in the order of 10^{-12} F cm^{-1} . $\text{LiTa}_{1-x}\text{Nb}_x\text{O}_3$ solid solution was of typical highly insulating material and the AC electrical conductivity was found to be temperature dependent. High dispersion behavior was observed for both

dielectric constants and losses at low frequency region and the electrical response became non-frequency dependent as frequency increased.

ACKNOWLEDGEMENTS

Special thanks are extended to the Research University Grant Scheme (RUGS), Universiti Putra Malaysia for the financial support.

REFERENCES

- Abrahams, S.C., Hamilton, W.C. & Reddy, J.M. 1966. Ferroelectric lithium niobate, single crystal neutron diffraction study. *Journal of Physics and Chemistry of Solids* 27: 1013-1018.
- Ballman, A.A. & Brown, H. 1972. Ferroelectric domain reversal in lithium metatantalate. *Ferroelectrics* 4: 189-194.
- Ekhelkar, S. & Bichile, G.K. 2004. Synthesis and characterization of $(\text{Bi}_2\text{O}_3)_{1-x}(\text{Y}_2\text{O}_3)_x$ and $(\text{Bi}_2\text{O}_3)_{1-x}(\text{Gd}_2\text{O}_3)_x$ solid solutions. *Bulletin of Material Science* 1: 19-22.
- Evans, C.R., Stanley, S.M., Percival, C.J., McHalea, G. & Newton, M.I. 2006. Lithium tantalate layer guided plate mode sensors. *Sensors and Actuators A* 132: 241-244.
- Gervais, F. & Fonseca, V. 1997. *Handbook of Optical Constants of Solids, Lithium Tantalate (LiTaO_3)*. Massachusetts: Academic Press. pp 777-805.
- Gopalan, V., Sanford, N.A., Aust, J.A., Kitamura, K. & Furukawa, Y. 2001. Crystal growth, characterization, and domain studies in lithium niobate and lithium tantalate ferroelectrics (Vol 4, Chapter 2). In *The Handbook of Advanced Electronic and Photonic Material and Devices*, edited by Hari Singh Nalwa. Massachusetts: Academic Press. pp. 57-114.
- Griffiths, P.R. & Haseth, J.A.D. 2007. Introduction to vibrational spectroscopy. In *Fourier Transform Infrared Spectroscopy*. Canada: John Wiley & Sons, Ltd. pp. 1-6.
- He, X., Li, K., Liu, M., He, Y., Zhang, X., Zhao, Y. & Xue, D. 2008. An optical spectroscopy study of defects in lithium tantalate single crystals. *Optics Communications* 281: 2531-2534.
- Hsu, R., Maslen, E.N. & Ishizawa, N. 1997. Synchrotron X-ray studies of LiNbO_3 and LiTaO_3 . *Acta Crystallographica, Section B: Structural Science* 53: 420.
- Irvine, J.T.S., Sinclair, D.C. & West, A.R. 1990. Electroceramics: Characterization by impedance spectroscopy. *Advanced Materials* 2: 132-138.
- Iyi, N., Kitamura, K., Izumi, F., Yamamoto, J. K., Hayashi, T., Asano, H. & Kimura, S. 1992. Comparative study of defect structures in lithium niobate with different compositions. *Journal of Solid State Chemistry* 101: 340-352.
- Kaczmarek, S.M., Swirkowicz, M., Jablonski, R., Lukasiewicz, T. & Kwasny, M. 2000. Growth and characterization of lithium tantalate single crystals doped with Ho, Tm, Nd, Yb, Pr and doped by diffusion with Cr and Cu. *Journal of Alloys and Compounds* 300-301: 322-328.
- Karhunen, T., Lahde, A., Leskinen, J., Buchel, R. & Waser, O. 2011. Transition metal-doped lithium titanium oxide nanoparticles made using flame spray pyrolysis. *ISRN Nanotechnology* 2001, Article ID 180821: 1-6.
- Khaw, C.C., Tan, K.B. & Lee, C.K. 2008. High temperature dielectric properties of cubic bismuth zinc tantalates. *Ceramics International* 35: 1473-1480.

- Kitamura, K., Yamamoto, J.K., Iyi, N. & Kirnura, S. 1992. Stoichiometric LiNbO₃ single crystal growth by double crucible Czochralski method using automatic power supply system. *Journal of Crystal Growth* 116: 327-332.
- Mark, L. 2001. Dielectric constant and loss tangent in LiNbO₃ crystals from 90 to 147 GHz. *Applied Physic Letters* 79: 1342-1345.
- Megaw, H.D. 1968. A note on the structure of lithium niobate, LiNbO₃. *Acta Crystallographica, Section A* 24: 583-588.
- Palatnikova, M.N., Biryukovaa, I.V., Sidorova, N.V., Denisovb, A.V., Kalinnikova, V.T., Smithc, P.G.R. & Shurd, V.Y. 2006. Growth and concentration dependencies of rare-earth doped lithium niobate single crystals. *Journal of Crystal Growth* 291: 390-397.
- Samuel, V., Gaikwad, A.B., Jadhav, A.D., Mirji, S.A. & Ravi, V. 2007. A novel technique to prepare LiNbO₃ at low temperature. *Materials Letters* 61: 765-766.
- Satapathy, S., Verma, P., Gupta, P.K., Mukherjee, C., Sathe, V.G. & Varma, K.B.R. 2011. Structural, dielectric and ferroelectric properties of multilayer lithium tantalate thin films prepared by sol-gel technique. *Thin Solid Films* 519: 1803-1808.
- Seshadri, R., Smith, M.B., Page, K. & Steigerwald, M.L. 2008. Crystal structure and the paraelectric-to-ferroelectric phase transition to nanoscale BaTiO₃. *Journal of the American Chemical Society* 130: 6955-6963.
- Tan, M.Y., Tan, K.B., Zainal, Z., Khaw, C.C. & Chen, S.K. 2012. Subsolidus formation and impedance spectroscopy studies of materials in the (Bi₂O₃)_{1-x}(Y₂O₃)_x binary system. *Ceramics International* 38: 3403-3409.
- Wachs, I.E., Briand, L.E., Jehng, J.M., Burcham, L. & Gao, X.T. 2000. Molecular structure and reactivity of the group V metal oxides. *Catalysis Today* 57: 323-330.
- Wan, Y., Guo, X., Chen, J., Yuan, X., Chu, J. & Li, J. 2002. Optical properties of nonlinear potassium lithium niobate crystal. *Journal of Crystal Growth* 235: 248-252.
- West, A.R. 1999. Crystal defects, non-stoichiometry and solid solutions. In *Solid State Chemistry and It Applications*. New Jersey: John Wiley & Sons, Ltd. pp 226-240.
- Xue, D., Betzler, K. & Hesse, H. 2000. Dielectric properties of lithium niobate tantalate crystals. *Solid State Communications* 115: 581-585.
- Yao, C.Y., Kao, T.H., Cheng, C.H. & Hurng, W.M. 1995. Studies of electrochemical properties of lithium cobalt oxide. *Journal of Power Sources* 54: 491-493.
- Zhan, J., Liu, D., Du, W., Wang, Z., Wang, P., Cheng, H., Huang, B. & Jiang, M. 2011. Synthesis and characterization of high crystallinity, well-defined morphology stoichiometric lithium niobate nanocrystalline. *Journal of Crystal Growth* 318: 1121-1124.

K.Y. Bak, K.B. Tan*, Z. Zainal, P.Y. Tan & M.P. Chon
 Department of Chemistry, Faculty of Science
 Universiti Putra Malaysia
 43400 Serdang, Selangor
 Malaysia

C.C. Khaw
 Department of Mechanical and Material Engineering
 Faculty of Engineering and Science
 Universiti Tunku Abdul Rahman
 53300 Setapak, Kuala Lumpur
 Malaysia

*Corresponding author; email: tankb@science.upm.my

Received: 21 August 2013

Accepted: 10 February 2014